Research Article | Vol. 13, No. 1 / 1 Jan 2022 / Biomedical Optics Express 374

Biomedical Optics EXPRESS

Single infrared light pulses induce excitatory and inhibitory neuromodulation

XUEDONG ZHU,[1,2,5] JEN-WEI LIN,[3] AHMET TURNALI,[4,5] AND MICHELLE Y. SANDER[1,2,4,5,6,*]

[1]Department of Biomedical Engineering, Boston University, 44 Cummington Mall, Boston, MA 02215, USA
[2]Neurophotonics Center, Boston University, 24 Cummington Mall, Boston, MA 02215, USA
[3]Department of Biology, Boston University, 5 Cummington Mall, Boston, MA 02215, USA
[4]Department of Electrical and Computer Engineering, Boston University, 8 Saint Mary's Street, Boston, MA 02215, USA
[5]Photonics Center, Boston University, 8 Saint Mary's Street, Boston, MA 02215, USA
[6]Division of Materials Science and Engineering, Boston University, 15 Saint Mary's Street, Brookline, MA 02446, USA
*msander@bu.edu

Abstract: The excitatory and inhibitory effects of single and brief infrared (IR) light pulses (2 μm) with millisecond durations and various power levels are investigated with a custom-built fiber amplification system. Intracellular recordings from motor axons of the crayfish opener neuromuscular junction are performed *ex vivo*. Single IR light pulses induce a membrane depolarization during the light pulses, which is followed by a hyperpolarization that can last up to 100 ms. The depolarization amplitude is dependent on the optical pulse duration, total energy deposition and membrane potential, but is insensitive to tetrodotoxin. The hyperpolarization reverses its polarity near the potassium equilibrium potential and is barium-sensitive. The membrane depolarization activates an action potential (AP) when the axon is near firing threshold, while the hyperpolarization reversibly inhibits rhythmically firing APs. In summary, we demonstrate for the first time that single and brief IR light pulses can evoke initial depolarization followed by hyperpolarization on individual motor axons. The corresponding mechanisms and functional outcomes of the dual effects are investigated.

1. Introduction

Infrared (IR) light pulses in the wavelength range of 1400 nm – 2100 nm have been used to stimulate or inhibit neural as well as muscular activities without chemical or genetic manipulation [1–6]. Advantages of IR neuromodulation (INM) over conventional electrical stimulation include high spatial-temporal selectivity and contactless delivery, minimizing potential physical intervention. Recent studies have demonstrated that INM can be combined with brain imaging techniques such as magnetic resonance imaging (MRI) [7] and optical coherence tomography (OCT) [8]. The compatibility has positioned INM at a promising position for basic and clinical brain research where simultaneous modulation and imaging are needed. Additional applications of INM range from brain stimulation [7,9–11], cochlear prostheses [12–14], and cardiac pacemakers [15] to neural identification and monitoring during surgery [16,17]. It is generally accepted that thermal transients induced by water and tissue absorption of pulsed IR light underlie the IR nerve stimulation (INS) [18,19] and IR nerve inhibition (INI) [20–22]. Heat-mediated nerve stimulation [23–25] and inhibition [26,27] have also been achieved with visible and near-IR light pulses by utilizing photo-active materials as extrinsic light absorbers and heat converters. With the photo-active materials being in contact with or attached to the target cell membrane, the light-induced heating is likely to be more spatially confined and with different temporal dynamics than those under direct IR light illumination. However, specifics of the biological processes

#444577 https://doi.org/10.1364/BOE.444577
Journal © 2022 Received 20 Oct 2021; revised 2 Dec 2021; accepted 6 Dec 2021; published 16 Dec 2021

Biomedical Optics EXPRESS

induced by these thermal transients under both the label-free and material-based techniques remain to be further examined.

In accordance with the photothermal effects, various mechanisms have been reported and discussed to explain INS [1]. Brief IR light pulses have been shown to evoke depolarization in multiple biological and artificial membranes. Changes in the membrane capacitive current resulting from alterations in the membrane structure caused by the IR light-induced spatiotemporal temperature gradients have been shown to generate depolarization [19,28–30]. Another proposed mechanism of INS, though less investigated, identified nanoporation in the plasma membrane caused by brief IR light pulses [31]. The nanopores result from the temporary destabilization of the plasma membrane and can act as channels for the flux of ions, which may depolarize cells or activate intracellular pathways [31,32]. The activation of heat-sensitive transient receptor potential vanilloid (TRPV) ion channels can also help explain INS observed in neurons or cells expressing these channels [33,34]. Finally, it has been suggested that IR light pulses can induce intracellular Ca^{2+} transients in a wide range of systems [9,35–39]. Though these Ca^{2+} transients exhibit relatively slow dynamics and are unlikely to directly generate action potentials (APs), they can indirectly alter neuronal excitability.

In contrast to INS, INI has been largely attributed to "heat block" effects [20–22,40–43]. Early studies using perfusion bath to raise bath temperature have shown that this manipulation can suppress the AP amplitude and duration or completely block APs [44,45]. These inhibitory effects stem from a combination of altered passive membrane properties and ion channel kinetics involved in generating APs. Accordingly, similar mechanisms have been assumed in INI. Specifically, increases in the cell membrane fluidity, which are correlated with a reduction in membrane resistance, can occur during and following short IR light pulses [46] and can lead to INI of AP initiation [22,43]. Moreover, successful modulation of AP waveforms and dynamics by IR light pulses suggests that temperature-dependent changes in K^+ and Na^+ channels kinetics are important contributors to INI [22,43,47]. Studies have also specifically emphasized the importance of tetraethylammonium (TEA)-sensitive and voltage-dependent K^+ ion channels for INI in *Aplysia* [41,42]. Overall, it is likely that the relative importance of the mechanisms outlined above may be neuron-specific.

Since the temperature rises induced by IR light pulses nonspecifically impact the passive membrane properties and ion channels, it is expected that both INS and INI effects can potentially be evoked concurrently or sequentially within neural tissues or even in a single neuron. Indeed, a silicon neural microdevice implanted into the rat cortical region both elevated and suppressed cortical multiunit responses to continuous wave (CW) IR light (1550 nm) irradiation [48]. Though the illumination regime with a pulse duration of 2 minutes was quite different from most INM reports, it nevertheless highlights the complex nature of INM, especially of the brain *in vivo*. So far, most INM studies have mainly focused on either INS or INI separately, rather than evaluating the net outcome of the two coexisting but opposite processes. For example, excitatory TRPV channels have been discussed extensively in INM studies [33,34,36–39,49]. However, heat-sensitive two-pore domain TWIK related K^+ (TREK) channels, which are known to be widely expressed among neurons and whose activation can generate inhibitory effects [50,51], have yet to be evaluated in INM. We believe that contributions of excitatory and inhibitory effects triggered by IR light pulses are likely to occur concurrently and should be considered together to realistically assess potentials of INM applications.

In this report, we use intracellular recordings to investigate both excitation and inhibition evoked by single and brief IR light (2 μm) pulses in single motor axons of the crayfish opener neuromuscular preparation. We examine biophysical processes underlying the dual effects and demonstrate for the first time that single and brief IR light pulses can excite or inhibit axonal APs in different functional contexts. Our data and exploration of the underlying mechanisms provide basic understanding of changes in the functional states of a neuron during INM. This

Biomedical Optics EXPRESS

study further establishes a foundation for predicting outputs generated by INM in more complex neural networks [7,11] and for translational applications [17].

2. Materials and methods

2.1. Infrared neuromodulation laser system

To systematically explore the effects of brief IR light pulses on the excitability of the motor axons, a custom-built high-power thulium-doped fiber amplifier (TDFA) was designed and constructed (Fig. 1(a)) that boosted the power of a 2-μm CW diode laser (FPL2000S, Thorlabs) up to 1 W. The thulium-doped double clad fiber (SM-TDF-10P/130-HE, Nufern) was used as a gain fiber for highly efficient operation between wavelengths of 1900–2100 nm. A 793-nm diode laser system (BWT Beijing Ltd., China) was used to pump the amplifier in a backward-pumping configuration. An acousto-optic modulator (AOM) (T-M250-0.3C16Z-3-F2P, Gooch & Housego) was incorporated into the setup after the amplification stage to shape clean pulses and to avoid unwanted background illumination resulting from amplified spontaneous emission. The AOM, which has a transmission rate of ~50% at 2 μm wavelength, was used to modulate the amplified output at the desired pulse duration and peak power.

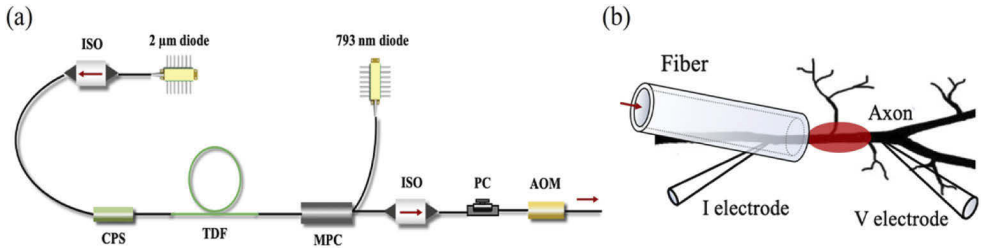

Fig. 1. Laser amplification system and electrophysiological setup. (a) Customized infrared neuromodulation laser system with custom-built thulium-doped fiber amplifier (TDFA). ISO, isolator; CPS, cladding power stripper; MPC, multimode pump coupler; PC, polarization controller; AOM, acousto-optic modulator. (b) Schematic representation of the electrophysiological configuration using two-electrode current clamp (TECC) to evaluate the IR light-mediated modulation of the motor axon. V electrode for voltage recording; I electrode for current stimulation.

The amplified 2 μm light was delivered to the target motor axon via an optical fiber with a core diameter of 105 μm, as shown in Fig. 1(b). For each preparation, the delivery fiber was positioned in line with the axon main branch, slightly above the axon surface at an angle of 28° to the horizontal plane. A red laser diode was coupled into the delivery fiber to facilitate the alignment. The delivery fiber was cleaved before each experiment and the power was measured at the free end of the delivery fiber. Single IR light pulses with various durations (0.2–10 ms) and average power levels (50–400 mW) were applied. The pulse energy ranged between 0.08–0.5 mJ/pulse. The resting membrane potential of the target axons was monitored during the recording. The stability of the resting membrane potential was used as the main criterion of a healthy axon [52]. Irreversible depolarization in the resting membrane potential was only observed when pulse energies significantly higher than 0.5 mJ/pulse were deposited.

2.2. Neuromuscular preparation and electrophysiological configuration

Crayfish (*Procambarus clarkii*) of both sexes were purchased from Niles Biological Supplies (Sacramento, CA). The opener neuromuscular preparation from the first pair of walking legs were dissected to expose both the inhibitory and the excitatory motor axons (20–30 μm in diameter) for this study. The control physiological saline contained (mM): 195 NaCl, 5.4 KCl, 13.5 $CaCl_2$, 2.6

Biomedical Optics EXPRESS

$MgCl_2$, 10 HEPES (pH 7.4). The saline was circulated by a peristaltic pump (Cole-Parmer, IL, USA) at a rate of around 1 ml/min during the recording. Two-electrode current clamp (TECC) recordings from the axon were performed with a MULTICLAMP 700B (Molecular Devices, CA, USA) and AXOCLAMP-2A (Axon Instruments Inc., CA, USA). Microelectrodes were filled with 0.5 mM KCl (40–60 MΩ). The recording electrode (voltage (V) electrode, Fig. 1(b)) was placed distal to the axon branch point, 350–400 μm away from the tip of the delivery fiber, to minimize the confounding effects of direct IR light illumination on electrodes. The stimulation electrode (current (I) electrode, Fig. 1(b)) was positioned on the axon main branch more proximal to the recording electrode. Both electrodes were arranged with an angle of ~28° to the horizontal plane. To monitor the IR light-induced temperature transients experienced by the target axons (see section S1 and Fig. S1 in Supplement 1), an open patch pipette filled with saline (~10 MΩ) was positioned slightly above the axon membrane and close to the illumination center. The electrophysiological recording was performed under an Olympus BX51 microscope with a 60X water immersion lens. All experiments were conducted at room temperature around 20–21 °C. All chemicals were purchased from Sigma-Aldrich unless specified otherwise.

2.3. Data analysis

Data acquisition and analysis were performed with Igor Pro (WaveMetrics). Voltage signals were filtered at 5 kHz and sampled at 50 kHz (NI USB-6363). Each preparation (N) represented a set of data recorded from an axon dissected from an animal. Statistical results were presented as average ± the standard error of mean (SEM) and the Student's t-test was used to determine the statistical significance with the significance level α set as 0.05.

3. Results

3.1. Brief infrared light pulses evoke axonal membrane potential depolarization followed by hyperpolarization

With the customized TDFA system depicted in Fig. 1(a), we first scanned for optimal duration-power combination that maximized depolarizing amplitude without tissue damage. Figures 2(a) – 2(d) illustrate membrane depolarizations evoked by IR light pulses of varying durations (0.2 ms – 10 ms) at four power levels. The axonal membrane potential (V_m) depolarized during the IR light pulses and decayed to resting level after the pulses. The decay descended into hyperpolarization in trials with higher energy levels. The amplitudes of the depolarization increased with increased power levels and durations (Figs. 2(a) – 2(d)). Results of the parameter scan is summarized by plotting the amplitudes of depolarization against the pulse duration for each power level (Fig. 2(e)). In general, the depolarization amplitude increased linearly with durations up to two milliseconds and plateaued as the pulse duration increased further. The bar plots in Fig. 2(f) summarize the depolarization amplitudes evoked by IR light pulses with the same energy level (0.4 mJ/pulse) for four pulse durations ($N = 8$). The depolarization amplitude was larger when the pulse energy was concentrated within shorter durations (see also the comparison in Fig. S2). Within the parameter space we scanned, the largest depolarization was achieved by a pulse of 1-ms duration with 400-mW power. For the rest of the study, IR light pulses of 400-mW average power and 1-ms duration were used for further investigation.

We also measured temperature transients, at the surface of motor axons, induced by the IR light pulse combinations used in Fig. 2. The local temperature increased rapidly during the IR light pulses and decayed to baseline within 100 ms (Fig. S1(a)). For the same pulse energy, higher peak temperature rises were achieved with shorter pulse durations (Fig. S1(a)) and the temperature rise increased as the total energy deposition went up (Fig. S1(b)). A maximum temperature rise of ~23°C was recorded for the 400-mW and 1-ms IR light pulses, which is comparable to measurements reported in previous studies [19,33]. The overall shapes of the temperature

Biomedical Optics EXPRESS

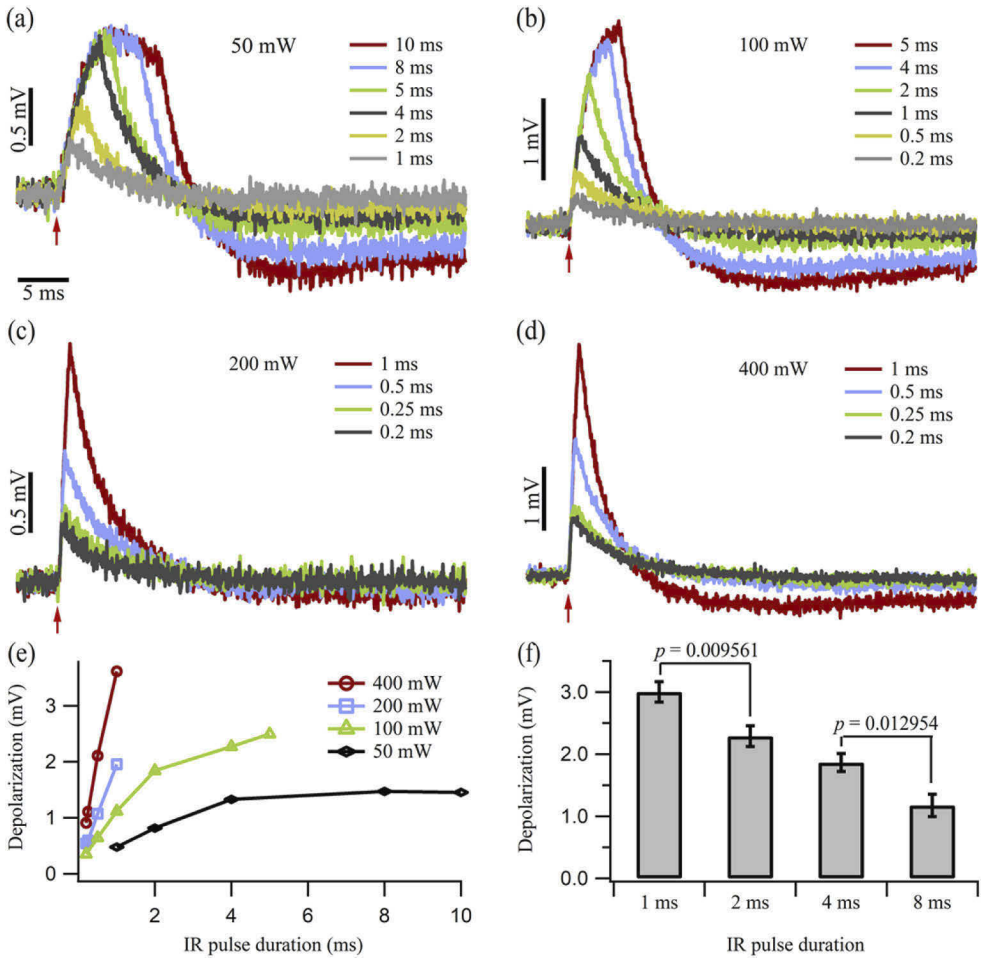

Fig. 2. Axonal membrane potential variations activated by brief and single IR light pulses. (a) – (d) Variations in axonal depolarization evoked by IR light pulses of varying durations and power levels. The red arrows indicate the starting point of the individual IR light pulses. The resting membrane potential was -68 mV, (a) – (d) share the same horizontal scale bar as shown in (a). (e) Depolarization amplitudes plotted against the IR light pulse duration for four different power levels. The amplitude was defined as the difference between the peak and baseline potential. The depolarization increased linearly when IR light pulses were less than 2 ms and plateaued as the pulse duration increased further. (f) Bar plot of the depolarization amplitude for four different pulse durations. For the same pulse energy (0.4 mJ/pulse), shorter IR light pulses resulted in larger depolarization. Data in (a) – (e) was recorded from one preparation and data in (f) was obtained from 8 preparations ($N = 8$) in total.

transients are similar to the V_m changes shown in Fig. 2, with two notable differences. First, the decay of the temperature transient is slower than that of the V_m. Whereas the temperature decayed to a low steady state ~50 ms after the IR light pulse, V_m typically had returned to baseline or undergone hyperpolarization by that time. Second, for the lower power level of 50 mW, the depolarization plateaued for durations longer than 4 ms (Fig. 2(e)) while the maximal temperature continued to rise for longer durations (Fig. S1(b)).

Biomedical Optics EXPRESS

3.2. Brief infrared light pulses-induced depolarization is tetrodotoxin-insensitive and voltage-dependent

In order to further characterize the IR light-induced depolarization, we first examined whether it was boosted by Na^+ influx. Figure 3(a) shows that the depolarizations remained unchanged before (dashed blue) and after (red) the Na^+ channel blocker tetrodotoxin (TTX) (200 nM) was applied. Thus, Na^+ channels did not bias the amplitude or duration of the depolarization ($p = 0.08684$, $N = 4$).

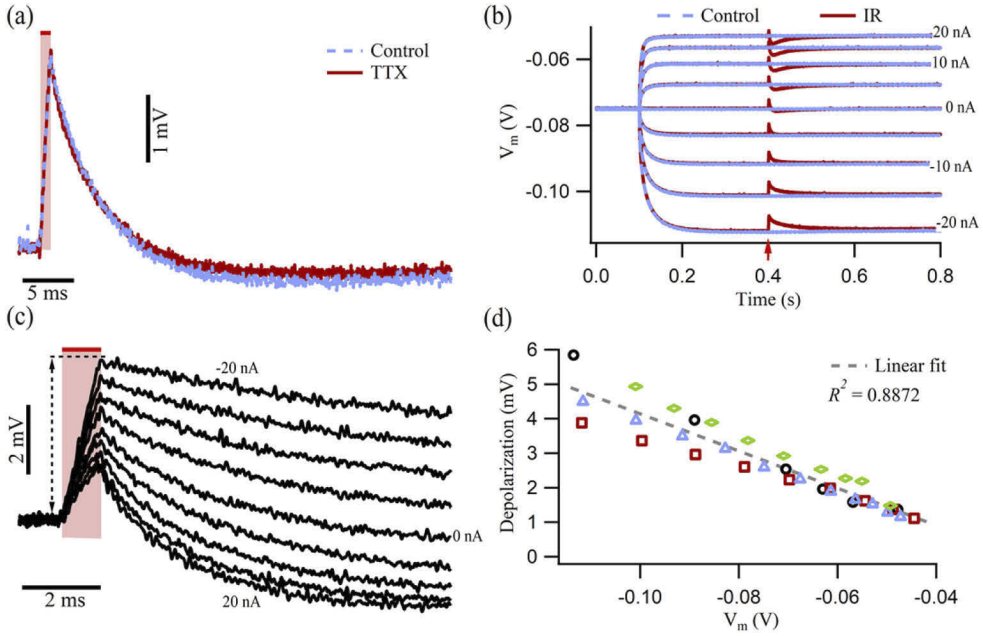

Fig. 3. Tetrodotoxin-insensitivity and voltage-dependence of IR light-induced membrane depolarization. (a) Comparison of the IR light-induced depolarization with (red) and without (dashed blue) 200 nM TTX. TTX did not change the depolarization amplitude. The red bar in (a) and (c) indicates the timing and duration of the IR light pulse (400 mW, 1 ms). (b) Membrane potential (V_m) recorded for nine current steps with (red) and without (dashed blue) IR light pulses (with 200 nM TTX and 10 μM ZD 7288 in presence). The red arrow indicates the starting point of the IR light pulses. Values on the right indicate the corresponding current levels, from -20 nA to 20 nA with a 5 nA step size. (c) IR light-induced depolarizations at different current steps with the depolarization and hyperpolarization highlighted. The dashed arrows indicate how the depolarization amplitudes were measured. (d) Voltage-dependence of IR light-induced depolarization. The amplitudes of the depolarization are plotted against the corresponding recorded V_m. A linear relationship ($R^2 = 0.8872$) can be established between the depolarization amplitude and the V_m, with a negative slope of -0.054. Different symbols represent recordings from different preparations ($N = 4$).

We next explored whether the IR light-induced depolarization exhibits any voltage dependence. The V_m of the target axon was shifted in both directions by a series of current steps delivered with a second intracellular stimulation electrode (Fig. 3(b)). V_m was recorded for nine different levels, with (red) and without (dashed blue) IR light pulses. The recordings were carried out in the presence of TTX (200 nM) and ZD 7288 (10 μM, Tocris), which were both added 20 min before the recordings. These two drugs linearize and expand the membrane polarization range for this study. TTX can inhibit the AP firing at large depolarization levels. ZD 7288 is a blocker of hyperpolarization-activated cation channels (I_h) which contribute to the resting membrane

Biomedical Optics EXPRESS

potential, input resistance as well as the "sag" during hyperpolarization (Fig. S3). As the current step went from -20 nA to 20 nA, the peak depolarization amplitude decreased while the hyperpolarization component became more noticeable. Subtracting the IR traces from the Control traces in Fig. 3(b) and aligning the baselines of the IR light-evoked potentials show the depolarization (and hyperpolarization) evolution clearly in Fig. 3(c). When the depolarizing amplitude was plotted against their corresponding V_m, a linear relationship with a slope of -0.054 was observed (Fig. 3(d), $R^2 = 0.8872$, $N = 4$). These results demonstrated that the membrane depolarization induced by short IR light pulses is voltage-sensitive and its amplitude decreases as the V_m depolarizes.

3.3. Brief infrared light pulses-induced hyperpolarization reverses its polarity near potassium equilibrium potential

A second and slower potential component of the IR light-induced membrane potential change could be observed following the initial and fast IR light-induced depolarization. The amplitude and polarity of this second component depended on the V_m. As shown in Fig. 3(b) (red), the second component was hyperpolarizing when the axon was depolarized and depolarizing when the axon was hyperpolarized. Given its physiological function illustrated below, we named the second component hyperpolarization based on its polarity at resting state and depolarized potentials. Figure 4(a) illustrates aligned traces recorded from different membrane potentials (from -100 mV to -40 mV). At resting membrane potential, the hyperpolarization in general lasted 50–100 ms. When the hyperpolarization amplitudes, measured at the time point of 7 ms after the IR light pulse, as indicated by the dashed gray line in Fig. 4(a), are plotted against the V_m biased by current injection, the hyperpolarization reversed around the resting membrane potential of -68 mV (Fig. 4(b), red cross). The reversal potential of the hyperpolarization shifted as the extracellular K^+ concentration ($[K^+]_o$) was varied, in the depolarizing direction for high $[K^+]_o$ and in the hyperpolarizing direction for low $[K^+]_o$ (Fig. 4(c)). While the actual reversal potential of the IR light induced-hyperpolarization varied considerably among different preparations, the dependence on $[K^+]_o$ examined in four preparations exhibited a consistent trend (Fig. 4(d)), which supports the hypothesis that the K^+ conductance likely contributed to the second component. For these measurements, 200 nM TTX and 10 μM ZD 7288 were used.

3.4. Barium-sensitive potassium channels contribute to the infrared light-induced hyperpolarization

We next aimed to explore the origin of the IR light-induced hyperpolarization. Based on the findings of the $[K^+]_o$-dependence of the hyperpolarization and its voltage-dependence (Fig. 4), we sought K^+ channels that are also heat-activated. The temperature-sensitive two-pore domain TWIK-related K^+ (TREK) channels satisfy both requirements [53]. More importantly, the IR-light induced temperature rises (Fig. S1) are within the window of the activation temperature (30–45°C) of TREK channels [50]. Thus, we tested this hypothesis by first examining the effects of a TREK channel blocker, Ba^{2+} (5 mM), on IR light-induced hyperpolarization (in the presence of TTX and ZD 7288). Consistent with the role of TREK channels in setting the resting membrane potential, the application of 5 mM Ba^{2+} depolarized the resting membrane potential (7.2 ± 0.47 mV ($N = 4$, $p = 0.00061$)) and increased the axonal membrane input resistance (Fig. 5(a), red). Ba^{2+}-mediated block of the IR light-induced hyperpolarization was apparent at depolarized V_m (red) (Fig. 5(b)). However, the blocking effects of Ba^{2+} appeared to be absent when the V_m was significantly hyperpolarized (Figs. 5(b) and 5(c)). This is consistent with previous studies showing that TREK channels exhibited a strong outward rectification, namely these channels were nearly impermeable to K^+ when the V_m was below the K^+ equilibrium potential [54–56]. On average, Ba^{2+} reduced the IR light-induced hyperpolarization amplitude by 61% ± 11% ($N = 4$, $p = 0.01044$) when +10 nA current steps were applied. Since the application of Ba^{2+}

Biomedical Optics EXPRESS

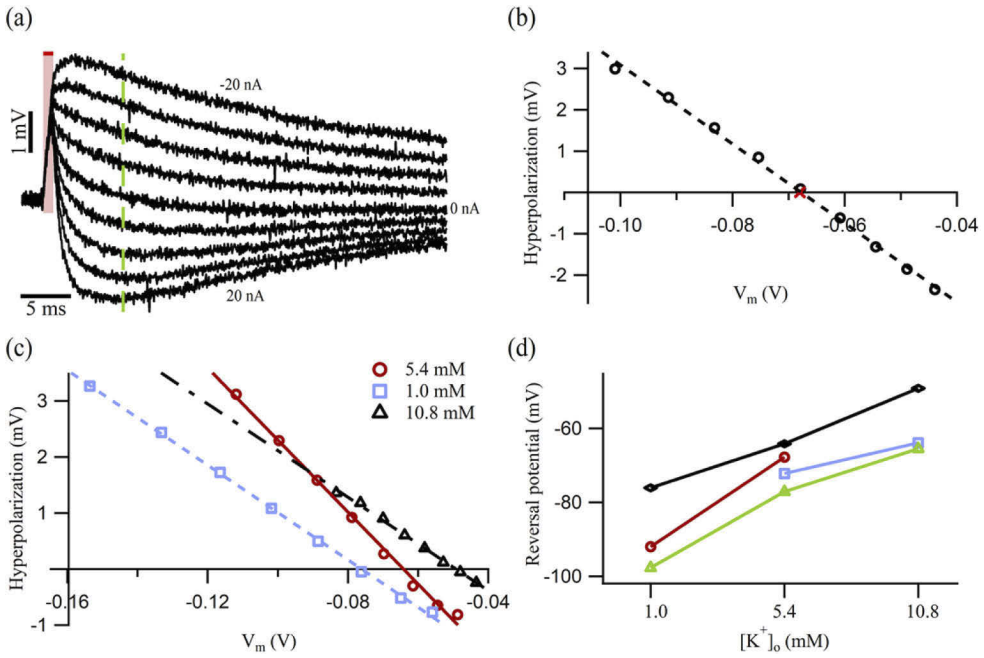

Fig. 4. Characterization of the IR light-induced hyperpolarization following the initial depolarization. (a) V_m variations at nine different current steps (5 nA step size) induced by IR light pulses (400 mW, 1 ms). The hyperpolarization recovered within 100 ms, depending on the V_m. The red bar indicates the timing and duration of the applied IR light pulse. The dashed green line indicates when the hyperpolarization amplitudes were measured for various current steps (or V_m levels). (b) The hyperpolarization amplitudes measured in (a) were plotted against the corresponding V_m at which they were recorded. The red cross shows the resting membrane potential (-68 mV). The hyperpolarization reversed around the resting membrane potential. (c) The voltage dependence of the hyperpolarization for three different extracellular K^+ concentrations ($[K^+]_o$). The $[K^+]_o$ was compensated with NaCl to maintain a constant extracellular osmolarity. (d) The reversal potential of the hyperpolarization depolarized as the $[K^+]_o$ increased and hyperpolarized with lower $[K^+]_o$, indicating a K^+ conductance contributing to the IR light-induced hyperpolarization ($p = 0.03535$ and 0.02654). Different symbols represent recordings from different preparations ($N = 4$).

also changed the resting membrane potential and input resistance of the axon, which could potentially lead to underestimation of the blockade, we further compared the K^+ conductance (g_K) underlying the IR light-induced hyperpolarization before and after Ba^{2+} application using the following equation:

$$g_K = \frac{\Delta V_h}{(V_m - E_{rv}) \cdot R_{in}}$$

Here, V_m is the membrane potential depolarized by +10 nA current steps, ΔV_h is the amplitude of the IR light-induced hyperpolarization measured using the V_m as the baseline, E_{rv} is the reversal potential of the IR light-induced hyperpolarization measured in control saline without Ba^{2+}, and R_{in} is the input resistance. V_m, ΔV_h, and R_{in} were measured separately before and after Ba^{2+} application. Under this condition, Ba^{2+} blocked 78% ± 6% ($N = 4$, $p = 0.00079$) of the g_K underlying the IR light-induced hyperpolarization (Fig. 5(c)). As the Ba^{2+}-sensitive TREK channels are outward rectifiers, the reversal potential of the hyperpolarization shifted to the right with Ba^{2+} (Fig. 5(d)). Ba^{2+} consistently right-shifted the reversal potential of the IR light-induced hyperpolarization by an average of 14.9 ± 1.68 mV ($N = 4$, $p = 0.00303$).

Biomedical Optics EXPRESS

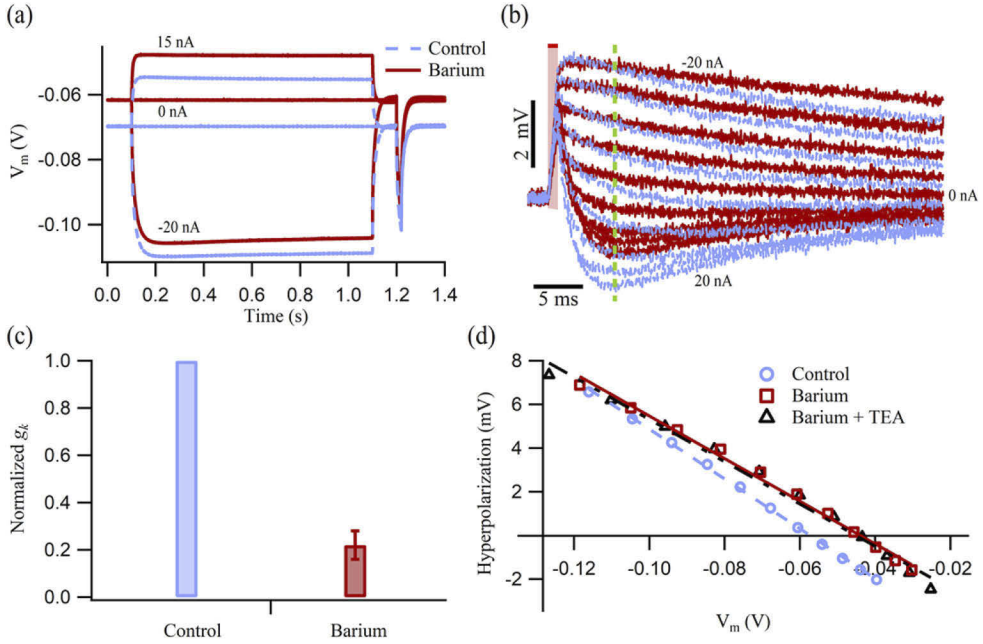

Fig. 5. Barium-sensitive K^+ ion channels contributed to the IR light-induced membrane hyperpolarization. (a) Example traces of V_m in response to 15 nA, 0 nA, and -20 nA current steps with (red) and without (dashed blue) 5 mM BCl_2 in the extracellular saline. Application of $BaCl_2$ depolarized the resting membrane potential by around 8 mV. (b) IR light-induced V_m variations with (red) and without (dashed blue) 5 mM $BaCl_2$. Blocks in the hyperpolarization were observed with the application of $BaCl_2$. The red bar indicates the timing and duration of the IR light pulse (400 mW, 1 ms). The dashed green line indicates when the hyperpolarization amplitudes were measured. (c) Application of 5 mM $BaCl_2$ reduced the g_K during the IR-light induced hyperpolarization by 78% ± 6% ($N = 4$, $p = 0.00079$) when +10 nA current steps were applied. (d) Voltage-dependence of the IR light-induced hyperpolarization without (circle) and with 5 mM $BaCl_2$ (rectangle) and 5 mM tetraethylammonium (TEA) (triangle). Barium reduced the hyperpolarization amplitude and shifted the reversal potential. Additional application of TEA (5 mM) did not further change the hyperpolarization.

The addition of 5 mM tetraethylammonium (TEA), a non-specific blocker of voltage-gated K^+ channels and Ca^{2+}-activated big K^+ (BK) channels, did not result in a further block (Fig. 5(d)). Reversing the order of the application of Ba^{2+} and TEA showed that TEA slightly reduced the amplitude of the hyperpolarization (Fig. S4), which may suggest a potential contribution from voltage-gated K^+ channels [41,42]. However, applying TEA first did not change the effectiveness of Ba^{2+} to significantly suppress the IR light-induced hyperpolarization (Fig. S4).

3.5. Single infrared light pulses facilitate AP generation and disrupt rhythmic AP firing

We next investigated the functional implications of the IR light-induced depolarization as well as hyperpolarization. Five preparations ($N = 5$) were used without any TTX or ZD 7288 treatment for this purpose. For the crayfish motor axon and the optical parameters adapted here, the maximum depolarization amplitude obtained at resting state was 3.0 ± 0.16 mV ($N = 8$), which was relatively small. The crayfish motor axon generally requires relatively large depolarization (10–15 mV) in order to fire APs. Indeed, we did not observe axonal AP firing induced solely by IR light pulses under the constraints of sub-damaging IR light intensity. However, in one of the

Biomedical Optics EXPRESS

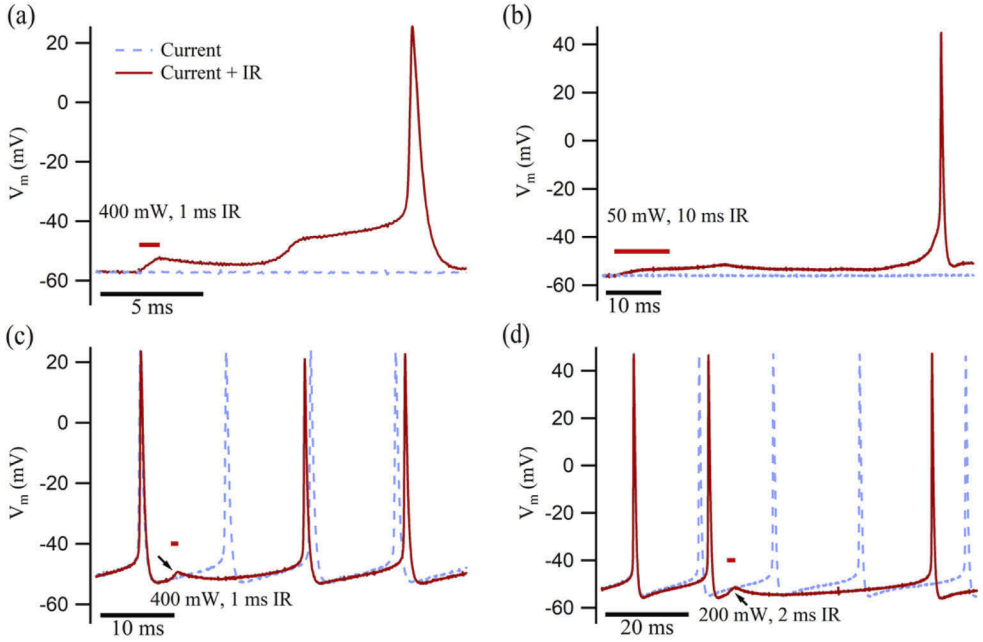

Fig. 6. Functional consequences of the depolarization and hyperpolarization induced by individual IR light pulses. (a), (b) With hybrid stimulation of subthreshold current steps (15 nA in (a) and 5 nA in (b)) and IR light pulses, the target axon successfully fired APs (red) following the IR light pulses. (c), (d) Single IR light pulses suppressed electrically-elicited AP generation. With suprathreshold current stimulation (20 nA in (c) and 15 nA in (d)), APs fired rhythmically. Application of a single IR light pulse reversibly suppressed the rhythm. The red bars indicate the timing and duration of IR light pulses. The arrows in (c) and (d) point out the IR light-induced initial depolarization.

five preparations, single IR light pulses successfully facilitated axonal AP generation (red) when the axonal V_m was depolarized by current injection just below the firing threshold, see Figs. 6(a) and 6(b). A delay in the onset of the AP firing was observed in both cases (Figs. 6(a) and 6(b)). The delay is likely a result from the interactions of the voltage-gated Na^+ and K^+ currents at near threshold membrane potentials, as well as the IR light-activated K^+ conductance. For the other four preparations, the IR light-induced depolarization, though not large enough to trigger AP firing, occurred during subthreshold current stimulation. On the other hand, when the axon was depolarized to a stable and rhythmic firing state, the application of a single IR light pulse reversibly disrupted the depolarizing trajectory between APs and suppressed AP firing during the time window of IR light induced hyperpolarization (Figs. 6(c) and 6(d)). The IR light-induced initial depolarization, though small, is visible as highlighted by the arrows. The reproducibility of the IR light-induced inhibition is illustrated in Fig. S5. The inhibition of AP firing was consistently observed with the five preparations tested. Collectively, the results demonstrate the functional relevance of the IR light induced depolarization and hyperpolarization in terms of AP firing.

4. Discussion

In this report, we used intracellular recordings from single axons to analyze the coexisting excitatory and inhibitory effects induced by single and brief IR light pulses. For excitation, we observed a TTX-independent depolarization whose amplitude was voltage-dependent (Fig. 3).

Biomedical Optics EXPRESS

This depolarization was more pronounced for shorter IR light pulses of higher pulse power (Fig. 2). The depolarization could trigger APs when axons were near their firing threshold (Figs. 6(a) and 6(b)). For inhibition, we showed a K^+ channel-mediated hyperpolarization that followed the initial depolarization and persisted up to 100 ms (Figs. 4 and 5). This hyperpolarization interrupted rhythmic AP firing by blocking APs (Figs. 6(c) and 6(d)). Pharmacological analysis suggested that TREK channels partially contributed to the IR light-mediated hyperpolarization.

These findings are complementary to our earlier reports on the modulatory effects of IR light pulses on AP initiation and propagation and downstream post synaptic activities [22,43]. In those studies, only inhibition in axonal excitability was observed when IR light pulses with significant longer pulse duration (up to 500 ms) and lower pulse power (7–13 mW) were applied to the same animal model used in this study. Collectively, they suggest that INM of neuronal excitability, while universal, largely depends on the physiological states of the target neurons, as well as on the parameters of the IR light pulses. Meanwhile, shorter IR light pulses are better suited to induce INS while longer pulses tend to lead to INI. Further, even for a model as simple as an individual axon, the INM outcomes are the net results of the INS and INI effects combined and thus INS and INI should be discussed not just individually but also collectively in INM studies. These considerations are critical to enhance our understanding of INM, especially for complex neural networks and tissues, and to enable further translational applications of INM.

4.1. Infrared light-induced membrane depolarization and its voltage-dependency

We observed a maximum depolarization from a resting state of ~3 mV induced by a single IR light pulse delivered by an optical fiber that illuminated a small part (~200 μm) of the crayfish motor axons. For the same total energy deposition, the larger depolarization amplitude was achieved with shorter pulse duration and higher pulse power (Figs. 2(e) and 2(f)). The depolarization component was TTX-insensitive (Fig. 3(a)), which agrees with the mechanism of IR light-induced membrane capacitance changes reported previously [19,28–30]. The results suggest that short IR light pulses of high pulse power are more efficient in terms of stimulating neurons with IR light-induced capacitive currents and should be preferred when achieving INS.

We also presented that the depolarization exhibited voltage-dependence: the amplitude decreased when the membrane potential was depolarized from -120 mV to -40 mV (Fig. 3(d)). This general trend of voltage-dependence of the IR light-induced depolarization is consistent with results using other preparations such as oocytes and HEK293T cells [19], mouse hair cells [28], neuromuscular junction of *Caenorhabditis elegans* [29], and rat dorsal root ganglion neurons [57]. However, values of the reversal potential varied considerably in these previous studies. For instance, the reversal potentials of the depolarization in oocytes and HEK293T cells were above +100 mV, while the reversal potential of the depolarization in cultured ganglion neurons, which are more comparable to our motor axons, was around -40 mV. This variation in reversal potentials could potentially be due to differences in the intracellular and extracellular ionic compositions and in the composition of the lipid molecules and other factors that can affect the membrane charge distributions [19,29]. The crayfish motor axons preclude adequate space clamp and thus a quantitative estimate of the reversal potential of the depolarization current is not possible. However, our *ex vivo* data was the first example obtained from peripheral axons and further demonstrated that IR light pulses can induce voltage-sensitive depolarizing current, which is independent of major membrane channel currents.

Functionally, we showed that IR light-induced depolarizations successfully triggered APs only when the target axons were near their firing threshold (Figs. 6(a) and 6(b)). It highlights a "selectivity" of INS, namely that only axons and neurons hovering around firing threshold can be synchronized by IR light pulses. The efficacy of the IR light-induced AP initiation reported here is similar to a previous study using oocytes co-expressing voltage-gated Na^+ and K^+ channels. In that study, the membrane potential of the transfected oocytes was depolarized to be within

Biomedical Optics EXPRESS

0.5–1 mV of their firing threshold in order for a single IR laser pulse to elicit an AP [19]. The large current step size (5 nA) we used in this study might have missed the membrane potential right below the firing threshold of target axons, thus led to a condition that was less favorable for observing IR light-evoked AP firing. While the small amplitudes of the depolarization seem limiting in its excitation capability, it is worth noting that only a small fraction of the target *ex vivo* crayfish motor axons and the transfected oocytes were illuminated. Expanding the area of illumination may increase the amplitude of the depolarization mediated by a capacitive current, though at the expense of decreased spatial selectivity. Moreover, functional consequences of the depolarization should be considered in the context that most mammalian central neurons are active spontaneously. Thus, a few millivolts depolarization can selectively stimulate cortical neurons that are already close to their firing threshold, while leaving other neurons unstimulated.

4.2. Infrared light-induced membrane hyperpolarization and the TREK channels

The photothermal heating generated by IR light pulses is expected to affect both the excitatory and the inhibitory components of the neurons and can thus induce opposite effects. In addition to the initial depolarizing current, a second hyperpolarization component was observed, which lasted up to 100 ms after the end of the IR light pulse. The amplitude and polarity of the hyperpolarization were found to be dependent on the membrane voltages (Figs. 4(a) and 4(b)). Our data suggests that g_K underlies the hyperpolarization, as the changes in $[K^+]_o$ shifted the reversal potential of the hyperpolarization in the direction predicted by the Nernst equilibration (Figs. 4(c) and 4(d)). This hyperpolarization, when applied to the target axons with suprathreshold stimulation, reversibly suppressed AP firing (Figs. 6(c) and 6(d)).

Two-pore domain potassium channels like TREK channels are known to exist in single-celled eukaryotes and above [58]. However, the more specific TREK channel types present in crayfish are unknown due to lack of genomic data. Nevertheless, pharmacological data with barium is consistent with the presence of TREK-type channels in the crayfish motor axons. The finding that the application of Ba^{2+} reduced 78% of the potassium conductance underlying the IR light-induced hyperpolarization strongly suggests that TREK-type K^+ channels contributed to the main component of the hyperpolarization. This partial reduction indicates that there were other players being activated by the IR light pulses. Given the diversity of ion channels expressed in different cell types, mechanisms underlying the hyperpolarization are likely to be cell specific [19,28,59]. In hair cells [28], for example, IR light-induced outward current was attributed to the voltage-activated delayed rectifier and BK-type channels activated by the IR light-evoked calcium influx and neurotransmitter release from efferent neurons. A previous study [60] using gold nanorods as photothermal transducers and near-infrared (785 nm) CW light as illumination source showed that TREK-1 activation contributed to thermally-mediated inhibition in cultured hippocampal neurons.

While effects of 5 mM Ba^{2+} described in this study strongly suggest that TREK channels may mediate the IR-light induced hyperpolarization, Ba^{2+} is known to also block other K^+ channels. We therefore also tested Spadin (Tocris), a TREK-1 specific blocker [56,61]. Spadin at 100 nM reduced the amplitude of the IR light-induced hyperpolarization at depolarized membrane potentials but to a smaller degree than 5 mM Ba^{2+} (Fig. S6). We believe that there are at least two reasons that could explain the smaller effects observed with Spadin (see section S2 in Supplement 1 for further explanations). Nevertheless, the observed Spadin effects are consistent with the importance of TREK channels in INM.

It is worth noting that TREK channels are widely expressed in mammalian brain [62,63]. Our data demonstrates and highlights the IR light-induced inhibitory role of TREK channels, which should be taken into account when applying and assessing INM. On the one hand, when brief IR light pulses are applied to neurons expressing TREK channels, TREK channel-mediated inhibition could occur simultaneously with other inhibitory effects that are due to heat-dependence

Biomedical Optics EXPRESS

of Na^+ and K^+ channel kinetics or passive membrane properties. These effects can work together to inhibit AP initiation and propagation. The duration of the TREK-mediated inhibition, which can be up to 100 ms following the initial depolarization, also provides a useful guidance in the selection of the frequency of IR light pulses if repetitive excitation is the goal. It suggests that the depolarization resulting from subsequent light pulses may occur during the hyperpolarization period activated by the previous light pulses if the pulse frequency is significantly higher than 10 Hz. On the other hand, in neurons not expressing TREK channels, depolarization generated by individual light pulses can be more effective in exciting neurons.

5. Conclusion

In summary, this study reported and systematically examined for the first time the coexisting excitatory and inhibitory effects as well as their functional significance that can be induced by a single and brief IR light pulse on an individual motor axon. The cellular events observed with intracellular recordings and the fundamental mechanisms explored here are likely to be common to most neurons exposed to IR light irradiation. Our findings offer critical perspectives into the understanding and application of INM. They suggest that the INM outcomes are largely the combined results of INS and INI, which further depend on the physiological states of the target neurons and the IR light pulse illumination regimes. They highlight the importance of the collective evaluation of INS and INI and the knowledge of heat-sensitive ion channels expressed in target neurons in order to better interpret and control INM.

Funding. Air Force Office of Scientific Research (FA9550-17-1-0276, FA9550-18-1-0348).

Disclosures. The authors declare no conflicts of interests.

Data availability. Data underlying the results presented in this paper are not publicly available at this time but may be obtained from the authors upon reasonable request.

Supplemental document. See Supplement 1 for supporting content.

References

1. Z. Fekete, Á. C. Horváth, and A. Zátonyi, "Infrared neuromodulation: a neuroengineering perspective," J. Neural Eng. **17**(5), 051003 (2020).
2. W. L. Hart, T. Kameneva, A. K. Wise, and P. R. Stoddart, "Biological considerations of optical interfaces for neuromodulation," Adv. Opt. Mater. **7**(19), 1900385 (2019).
3. K. Zhao, X. Tan, H. Young, and C.-P. Richter, "Stimulation of neurons with infrared radiation," in *Biomedical Optics in Otorhinolaryngology: Head and Neck Surgery*, B. J.-F. Wong and J. Ilgner, eds. (Springer, 2016), pp. 253–284.
4. C.-P. Richter and X. Tan, "Photons and neurons," Hear. Res. **311**, 72–88 (2014).
5. M. Chernov and A. W. Roe, "Infrared neural stimulation: a new stimulation tool for central nervous system applications," Neurophoton **1**, 011011 (2014).
6. C.-P. Richter, A. I. Matic, J. D. Wells, E. D. Jansen, and J. T. Walsh, "Neural stimulation with optical radiation," Laser & Photon. Rev. **5**(1), 68–80 (2011).
7. A. G. Xu, M. Qian, F. Tian, B. Xu, R. M. Friedman, J. Wang, X. Song, Y. Sun, M. M. Chernov, J. M. Cayce, E. D. Jansen, A. Mahadevan-Jansen, X. Zhang, G. Chen, and A. W. Roe, "Focal infrared neural stimulation with high-field functional MRI: a rapid way to map mesoscale brain connectomes," Sci. Adv. **5**(4), eaau7046 (2019).
8. Y. Zhang, L. Yao, F. Yang, S. Yang, A. Edathodathil, W. Xi, A. W. Roe, and P. Li, "INS-fOCT: a label-free, all-optical method for simultaneously manipulating and mapping brain function," Neurophoton. **7**, 015014 (2020).
9. J. M. Cayce, M. B. Bouchard, M. M. Chernov, B. R. Chen, L. E. Grosberg, E. D. Jansen, E. M. C. Hillman, and A. Mahadevan-Jansen, "Calcium imaging of infrared-stimulated activity in rodent brain," Cell Calcium **55**(4), 183–190 (2014).
10. J. M. Cayce, R. M. Friedman, E. D. Jansen, A. Mahavaden-Jansen, and A. W. Roe, "Pulsed infrared light alters neural activity in rat somatosensory cortex in vivo," NeuroImage **57**(1), 155–166 (2011).
11. J. M. Cayce, R. M. Friedman, G. Chen, E. D. Jansen, A. Mahadevan-Jansen, and A. W. Roe, "Infrared neural stimulation of primary visual cortex in non-human primates," NeuroImage **84**, 181–190 (2014).
12. S. M. Rajguru, A. I. Matic, A. M. Robinson, A. J. Fishman, L. E. Moreno, A. Bradley, I. Vujanovic, J. Breen, J. D. Wells, M. Bendett, and C.-P. Richter, "Optical cochlear implants: Evaluation of surgical approach and laser parameters in cats," Hear. Res. **269**(1-2), 102–111 (2010).
13. Y. Xu, N. Xia, M. Lim, X. Tan, M. H. Tran, E. Boulger, F. Peng, H. Young, C. Rau, A. Rack, and C.-P. Richter, "Multichannel optrodes for photonic stimulation," Neurophoton. **5**, 045002 (2018).

Biomedical Optics EXPRESS

14. A. C. Thompson, J. B. Fallon, A. K. Wise, S. A. Wade, R. K. Shepherd, and P. R. Stoddart, "Infrared neural stimulation fails to evoke neural activity in the deaf guinea pig cochlea," Hear. Res. **324**, 46–53 (2015).
15. S. M. Ford, M. Watanabe, and M. W. Jenkins, "A review of optical pacing with infrared light," J. Neural Eng. **15**(1), 011001 (2018).
16. N. M. Fried, S. Rais-Bahrami, G. A. Lagoda, A.-Y. Chuang, L.-M. Su, and A. L. Burnett III, "Identification and imaging of the nerves responsible for erectile function in rat prostate, in vivo, using optical nerve stimulation and optical coherence tomography," IEEE J. Sel. Top. Quantum Electron. **13**(6), 1641–1645 (2007).
17. J. M. Cayce, J. D. Wells, J. D. Malphrus, C. Kao, S. Thomsen, N. B. Tulipan, P. E. Konrad, E. D. Jansen, and A. Mahadevan-Jansen, "Infrared neural stimulation of human spinal nerve roots *in vivo*," Neurophotonics **2**(1), 015007 (2015).
18. J. Wells, C. Kao, P. Konrad, T. Milner, J. Kim, A. Mahadevan-Jansen, and E. D. Jansen, "Biophysical mechanisms of transient optical stimulation of peripheral nerve," Biophys. J. **93**(7), 2567–2580 (2007).
19. M. G. Shapiro, K. Homma, S. Villarreal, C.-P. Richter, and F. Bezanilla, "Infrared light excites cells by changing their electrical capacitance," Nat. Commun. **3**(1), 736 (2012).
20. Z. Mou, I. F. Triantis, V. M. Woods, C. Toumazou, and K. Nikolic, "A simulation study of the combined thermoelectric extracellular stimulation of the sciatic nerve of the xenopus laevis: the localized transient heat block," IEEE Trans. Biomed. Eng. **59**(6), 1758–1769 (2012).
21. A. R. Duke, M. W. Jenkins, H. Lu, J. M. McManus, H. J. Chiel, and E. D. Jansen, "Transient and selective suppression of neural activity with infrared light," Sci Rep **3**(1), 2600 (2013).
22. X. Zhu, J.-W. Lin, and M. Y. Sander, "Infrared inhibition and waveform modulation of action potentials in the crayfish motor axon," Biomed. Opt. Express **10**, 6580–6594 (2019).
23. K. Eom, J. Kim, J. M. Choi, T. Kang, J. W. Chang, K. M. Byun, S. B. Jun, and S. J. Kim, "Enhanced infrared neural stimulation using localized surface plasmon resonance of gold nanorods," Small **10**(19), 3853–3857 (2014).
24. J. L. Carvalho-de-Souza, J. S. Treger, B. Dang, S. B. H. Kent, D. R. Pepperberg, and F. Bezanilla, "Photosensitivity of neurons enabled by cell-targeted gold nanoparticles," Neuron **86**(1), 207–217 (2015).
25. J. L. Carvalho-de-Souza, B. I. Pinto, D. R. Pepperberg, and F. Bezanilla, "Optocapacitive generation of action potentials by microsecond laser pulses of nanojoule energy," Biophys. J. **114**(2), 283–288 (2018).
26. P. Feyen, E. Colombo, D. Endeman, M. Nova, L. Laudato, N. Martino, M. R. Antognazza, G. Lanzani, F. Benfenati, and D. Ghezzi, "Light-evoked hyperpolarization and silencing of neurons by conjugated polymers," Sci Rep **6**(1), 22718 (2016).
27. S. Yoo, J.-H. Park, and Y. Nam, "Single-cell photothermal neuromodulation for functional mapping of neural networks," ACS Nano **13**(1), 544–551 (2019).
28. R. D. Rabbitt, A. M. Brichta, H. Tabatabaee, P. J. Boutros, J. Ahn, C. C. Della Santina, L. A. Poppi, and R. Lim, "Heat pulse excitability of vestibular hair cells and afferent neurons," Journal of Neurophysiology **116**(2), 825–843 (2016).
29. Q. Liu, M. J. Frerck, H. A. Holman, E. M. Jorgensen, and R. D. Rabbitt, "Exciting cell membranes with a blustering heat shock," Biophysical Journal **106**(8), 1570–1577 (2014).
30. M. Plaksin, E. Shapira, E. Kimmel, and S. Shoham, "Thermal transients excite neurons through universal intramembrane mechanoelectrical effects," Phys. Rev. X **8**, 011043 (2018).
31. H. T. Beier, G. P. Tolstykh, J. D. Musick, R. J. Thomas, and B. L. Ibey, "Plasma membrane nanoporation as a possible mechanism behind infrared excitation of cells," J. Neural Eng. **11**(6), 066006 (2014).
32. A. G. Pakhomov, A. M. Bowman, B. L. Ibey, F. M. Andre, O. N. Pakhomova, and K. H. Schoenbach, "Lipid nanopores can form a stable, ion channel-like conduction pathway in cell membrane," Biochem. Biophys. Res. Commun. **385**(2), 181–186 (2009).
33. J. Yao, B. Liu, and F. Qin, "Rapid temperature jump by infrared diode laser irradiation for patch-clamp studies," Biophys. J. **96**(9), 3611–3619 (2009).
34. E. S. Albert, J. M. Bec, G. Desmadryl, K. Chekroud, C. Travo, S. Gaboyard, F. Bardin, I. Marc, M. Dumas, G. Lenaers, C. Hamel, A. Muller, and C. Chabbert, "TRPV4 channels mediate the infrared laser-evoked response in sensory neurons," J. Neurophysiol. **107**(12), 3227–3234 (2012).
35. G. M. Dittami, S. M. Rajguru, R. A. Lasher, R. W. Hitchcock, and R. D. Rabbitt, "Intracellular calcium transients evoked by pulsed infrared radiation in neonatal cardiomyocytes," The Journal of Physiology **589**(6), 1295–1306 (2011).
36. V. Lumbreras, E. Bas, C. Gupta, and S. M. Rajguru, "Pulsed infrared radiation excites cultured neonatal spiral and vestibular ganglion neurons by modulating mitochondrial calcium cycling," J. Neurophysiol. **112**(6), 1246–1255 (2014).
37. J. N. Barrett, S. Rincon, J. Singh, C. Matthewman, J. Pasos, E. F. Barrett, and S. M. Rajguru, "Pulsed infrared releases Ca^{2+} from the endoplasmic reticulum of cultured spiral ganglion neurons," J. Neurophysiol. **120**(2), 509–524 (2018).
38. D. Moreau, C. Lefort, J. Pas, S. M. Bardet, P. Leveque, and R. P. O'Connor, "Infrared neural stimulation induces intracellular Ca^{2+} release mediated by phospholipase C," J. Biophotonics **11**(2), e201700020 (2018).
39. A. I. Borrachero-Conejo, W. R. Adams, E. Saracino, M. G. Mola, M. Wang, T. Posati, F. Formaggio, M. D. Bellis, A. Frigeri, M. Caprini, M. R. Hutchinson, M. Muccini, R. Zamboni, G. P. Nicchia, A. Mahadevan-Jansen, and V. Benfenati, "Stimulation of water and calcium dynamics in astrocytes with pulsed infrared light," The FASEB Journal **34**(5), 6539–6553 (2020).

Biomedical Optics EXPRESS

40. E. H. Lothet, K. M. Shaw, H. Lu, J. Zhuo, Y. T. Wang, S. Gu, D. B. Stolz, E. D. Jansen, C. C. Horn, H. J. Chiel, and M. W. Jenkins, "Selective inhibition of small-diameter axons using infrared light," Sci Rep **7**(1), 3275 (2017).
41. M. Ganguly, M. W. Jenkins, E. D. Jansen, and H. J. Chiel, "Thermal block of action potentials is primarily due to voltage-dependent potassium currents: a modeling study," J. Neural Eng. **16**(3), 036020 (2019).
42. M. Ganguly, J. B. Ford, J. Zhuo, M. T. McPheeters, M. W. Jenkins, H. J. Chiel, and E. D. Jansen, "Voltage-gated potassium channels are critical for infrared inhibition of action potentials: an experimental study," Neurophotonics **6**(04), 1 (2019).
43. X. Zhu, J.-W. Lin, and M. Y. Sander, "Infrared inhibition impacts on locally initiated and propagating action potentials and the downstream synaptic transmission," Neurophoton. **7**, 045003 (2020).
44. A. L. Hodgkin and B. Katz, "The effect of temperature on the electrical activity of the giant axon of the squid," The Journal of Physiology **109**(1-2), 240–249 (1949).
45. B. Frankenhaeuser and L. E. Moore, "The effect of temperature on the sodium and potassium permeability changes in myelinated nerve fibres of Xenopus laevis," The Journal of Physiology **169**(2), 431–437 (1963).
46. A. J. Walsh, J. C. Cantu, B. L. Ibey, and H. T. Beier, "Short infrared laser pulses increase cell membrane fluidity," Proc. SPIE **10062**, 100620D (2017).
47. G. P. Tolstykh, B. L. Ibey, A. V. Sedelnikova, C. M. Valdez, J. C. Cantu, and I. Echchgadda, "Infrared laser-induced fast thermal gradient affects the excitability of primary hippocampal neurons," Proc. SPIE **11238**, 112380Z 2020).
48. Á. C. Horváth, S. Borbély, Ö. C. Boros, L. Komáromi, P. Koppa, P. Barthó, and Z. Fekete, "Infrared neural stimulation and inhibition using an implantable silicon photonic microdevice," Microsyst Nanoeng **6**(1), 44 (2020).
49. L. Paris, I. Marc, B. Charlot, M. Dumas, J. Valmier, and F. Bardin, "Millisecond infrared laser pulses depolarize and elicit action potentials on in-vitro dorsal root ganglion neurons," Biomed. Opt. Express **8**, 4568–4578 (2017).
50. J. A. Lamas, L. Rueda-Ruzafa, and S. Herrera-Pérez, "Ion channels and thermosensitivity: TRP, TREK, or both?" Int. J. Mol. Sci. **20**(10), 2371 (2019).
51. A. D. Medhurst, G. Rennie, C. G. Chapman, H. Meadows, M. D. Duckworth, R. E. Kelsell, I. I. Gloger, and M. N. Pangalos, "Distribution analysis of human two pore domain potassium channels in tissues of the central nervous system and periphery," Mol. Brain Res. **86**(1-2), 101–114 (2001).
52. W. G. A. Brown, K. Needham, J. M. Begeng, A. C. Thompson, B. A. Nayagam, T. Kameneva, and P. R. Stoddart, "Thermal damage threshold of neurons during infrared stimulation," Biomed. Opt. Express **11**, 2224–2234 (2020).
53. E. R. Schneider, E. O. Anderson, E. O. Gracheva, and S. N. Bagriantsev, "Chapter five - temperature sensitivity of two-pore (K2P) potassium channels," in *Current Topics in Membranes*, L. D. Islas and F. Qin, eds., Thermal Sensors (Academic Press, 2014), Vol. 74, pp. 113–133.
54. K. J. Ford, D. A. Arroyo, J. N. Kay, E. E. Lloyd, R. M. Bryan, J. R. Sanes, and M. B. Feller, "A role for TREK1 in generating the slow afterhyperpolarization in developing starburst amacrine cells," J. Neurophysiol. **109**(9), 2250–2259 (2013).
55. A. Cadaveira-Mosquera, S. J. Ribeiro, A. Reboreda, M. Pérez, and J. A. Lamas, "Activation of TREK currents by the neuroprotective agent riluzole in mouse sympathetic neurons," J. Neurosci. **31**(4), 1375–1385 (2011).
56. R. Ma and A. Lewis, "Spadin selectively antagonizes arachidonic acid activation of TREK-1 channels," Front. Pharmacol. **11**, 434 (2020).
57. E. J. Katz, I. K. Ilev, V. Krauthamer, D. H. Kim, and D. Weinreich, "Excitation of primary afferent neurons by near-infrared light in vitro," NeuroReport **21**(9), 662–666 (2010).
58. T. J. Jegla, C. M. Zmasek, S. Batalov, and S. K. Nayak, "Evolution of the human ion channel set," Comb. Chem. High Throughput Screening **12**(1), 2–23 (2009).
59. N. Martino, P. Feyen, M. Porro, C. Bossio, E. Zucchetti, D. Ghezzi, F. Benfenati, G. Lanzani, and M. R. Antognazza, "Photothermal cellular stimulation in functional bio-polymer interfaces," Sci. Rep. **5**(1), 8911 (2015).
60. S. Yoo, S. Hong, Y. Choi, J.-H. Park, and Y. Nam, "Photothermal inhibition of neural activity with near-infrared-sensitive nanotransducers," ACS Nano **8**(8), 8040–8049 (2014).
61. J. Mazella, O. Pétrault, G. Lucas, E. Deval, S. Béraud-Dufour, C. Gandin, M. El-Yacoubi, C. Widmann, A. Guyon, E. Chevet, S. Taouji, G. Conductier, A. Corinus, T. Coppola, G. Gobbi, J.-L. Nahon, C. Heurteaux, and M. Borsotto, "Spadin, a sortilin-derived peptide, targeting rodent TREK-1 channels: a new concept in the antidepressant drug design," PLoS Biol. **8**(4), e1000355 (2010).
62. M. Lengyel, P. Enyedi, and G. Czirják, "Negative influence by the force: mechanically induced hyperpolarization via k2p background potassium channels," Int. J. Mol. Sci. **22**(16), 9062 (2021).
63. M. Fink, F. Duprat, F. Lesage, R. Reyes, G. Romey, C. Heurteaux, and M. Lazdunski, "Cloning, functional expression and brain localization of a novel unconventional outward rectifier K+ channel," The EMBO Journal **15**(24), 6854–6862 (1996).